Research Article | Vol. 27, No. 10 | 13 May 2019 | OPTICS EXPRESS 14353

Optics EXPRESS

Self-steering partially coherent vector beams

HAIDAN MAO,[1] YAHONG CHEN,[2,6] CHUNHAO LIANG,[2,3] LINFEI CHEN,[1] YANGJIAN CAI,[2,4,7] AND SERGEY A. PONOMARENKO[3,5]

[1]*School of Science, Hangzhou Dianzi University, Hangzhou 310018, China*
[2]*School of Physical Science and Technology, Soochow University, Suzhou 215006, China*
[3]*Department of Electrical and Computer Engineering, Dalhousie University, Halifax, Nova Scotia B3J 2X4, Canada*
[4]*Shandong Provincial Engineering and Technical Center of Light Manipulations & Shandong Provincial Key Laboratory of Optics and Photonic Device, School of Physics and Electronics, Shandong Normal University, Jinan 250014, China*
[5]*Department of Physics and Atmospheric Science, Dalhousie University, Halifax, Nova Scotia B3H 4R2, Canada*
[6]*yahongchen@suda.edu.cn*
[7]*yangjiancai@suda.edu.cn*

Abstract: We introduce a class of self-steering partially coherent vector optical beams with the aid of a generalized complex Gaussian representation. We show that such partially coherent vector beams have mobile guiding centers of their intensity and polarization state distributions on the beam free space propagation that could be employed to generate far-field polarization arrays. Further, we introduce theoretically and realize experimentally a class of vector beams with inhomogeneous statistical and nontrivial far-field angular distributions, which we term cylindrically correlated partially coherent (CCPC) vector beams. We find that such novel beams possess, in general, cylindrically polarized, far-field patterns of an adjustable degree of polarization. The steering control of the intensity and polarization of the self-steering CCPC vector beam is also demonstrated in experiment. Our findings can find important applications, such as trapping of neutral microparticles and excitation of novel surface waves.

1. Introduction

Optical coherence, as one of the fundamental properties of light, plays an important role in the light field manipulation and the light-matter interactions [1]. Recent studies have shown that the light coherence structure can be viewed as an indispensable degree of freedom to control the physical properties of propagating beams [2–9] and surface waves, from evanescent waves [10] to surface plasmon polaritons [11–15]. Several types of partially coherent fields with statistically nonuniform correlation functions have been introduced and generated via various coherence manipulation methods [16–21]. These fields exhibit many interesting properties during propagation such as self-splitting, self-focusing, and self-shaping in either space or time domains [2,4–9,22–25], and are envisioned useful in a wealth of applications to free-space optical communications [26,27], super-resolution imaging [28,29], and longitudinal field shaping [30]. Phase structuring of the complex coherence function has also been introduced recently [31–35], and has shown the ability to modulate the propagation dynamics and far-field intensities of the optical beams [36]. In particular, self-steering partially coherent beams have been lately introduced by appropriate phase engineering of the cross-spectral density of a partially coherent source [32]. Such beams possess a moving guiding center and they maintain their cross-spectral density shape on free space propagation. The self-steering partially coherent beams can find applications to trapped particle transport and mobile target tracing.

Polarization is another fundamental feature of light fields, reflecting their vector nature. Until recently, coherence and polarization of light fields had been treated separately for historical

#355766 https://doi.org/10.1364/OE.27.014353
Journal © 2019 Received 19 Dec 2018; revised 16 Mar 2019; accepted 26 Apr 2019; published 3 May 2019

reasons [37]. In 1994, James predicted theoretically that the degree of polarization of a partially coherent beam can change on propagation in even free space [38]. This was subsequently verified experimentally by Vidal *et al.* in 2011 [39]. Since Gori in 1998 [40] and Wolf in 2003 [41] developed unified theories of coherence and polarization for the random electromagnetic beams in time and frequency domains, respectively, numerous studies have been devoted to partially coherent vector beams aiming to elucidate their fundamental properties and outline potential applications [42–44]. After Gori *et al.* [45] introduced a sufficient condition for devising bona fide cross-spectral density matrices of optical sources, increasing attention has been paid to the spatial coherence structure engineering of partially coherent vector beams. In 2014, Chen *et al.* introduced a class of nonuniformly correlated partially coherent vector beams [46]. A fully polarized intensity fraction of such beams is radially polarized in the far zone of the source. As the source spatial coherence decreases, a very pure radially polarized, partially coherent far field can be generated by the source, a feature combination especially conducive to reliable particle trapping [47] and material thermal processing applications [48].

In this paper, we extend the concept of self-steering partially coherent *scalar* beams to the *electromagnetic (vector)* domain by using a generalized complex Gaussian representation for the cross-spectral density matrices. Such self-steering vector beams possess a dynamic guiding center of their intensity and Stokes parameter profiles as the beams propagate in free space. To illustrate our general formalism, we introduce both theoretically and experimentally a class of partially coherent vector beams with nonuniform correlations and nontrivial far-field features that we term cylindrically correlated partially coherent (CCPC) vector beams. We find that such CCPC vector beams can create cylindrically polarized far fields of any degree of polarization. We further put forward the experiment to generate the self-steering CCPC vector beam and demonstrate its dynamic propagation properties.

2. Generalized complex Gaussian representation of partially coherent vector beams

The complex Gaussian representation (CGR) of *scalar* partially coherent fields was introduced by Ponomarenko [49] by analogy with the Glauber-Sudarshan P-representation of quantum optics [1]. According to the CGR, a partially coherent field can be expressed as a linear superposition of uncorrelated and phase-shifted complex Gaussian modes, which can be routinely produced in the laboratory using standard lasers as light sources. Therefore, the CGR opens up alternative avenues for coherence structure engineering and novel partially coherent source design. The optical coherence lattices and gratings with periodic spatial and temporal coherence properties have been constructed with the help of the CGR [31,50]. Moreover, the CGR provides a convenient approach for dealing with partially coherent fields propagation through various systems, such as free space [36], graded-index media [51], the turbulent atmosphere [52], and uniaxial crystals [53]. In this section, we will introduce a generalized CGR of partially coherent vector beams, and apply it to examine partially coherent vector beam propagation through generic optical ABCD systems.

2.1. Representation

The statistical properties of a partially coherent vector beam, propagating close to the optical axis (i.e., along z-axis), are characterized by a 2×2 (space-frequency) cross-spectral density matrix or (space-time) coherence-polarization matrix. In the space-frequency domain, the cross-spectral density matrix at the source plane ($z = 0$) can be written as [44]

$$\mathbf{W}(\mathbf{r}_1, \mathbf{r}_2, 0) = \begin{bmatrix} W_{xx}(\mathbf{r}_1, \mathbf{r}_2, 0) & W_{xy}(\mathbf{r}_1, \mathbf{r}_2, 0) \\ W_{yx}(\mathbf{r}_1, \mathbf{r}_2, 0) & W_{yy}(\mathbf{r}_1, \mathbf{r}_2, 0) \end{bmatrix}, \tag{1}$$

Optics EXPRESS

with the elements

$$W_{mn}(\mathbf{r}_1, \mathbf{r}_2, 0) = \langle E_m^*(\mathbf{r}_1) E_n(\mathbf{r}_2) \rangle, \tag{2}$$

where $(m, n) \in (x, y)$, $\mathbf{r}_1 \equiv (x_1, y_1)$ and $\mathbf{r}_2 \equiv (x_2, y_2)$ are two arbitrary position vectors in the source plane, E_x and E_y denote the components of a random electric field along two mutually orthogonal x and y directions perpendicular to the z axis. The asterisk and the angular brackets denote the complex conjugate and ensemble average, respectively. Hereafter, we omit the angular frequency ω for simplicity.

A straightforward CGR extension to the vectorial case implies that the cross-spectral density matrix for any partially coherent vector fields can be represented as

$$\mathbf{W}(\mathbf{R}_1, \mathbf{R}_2, 0) = \int \mathrm{d}^4\boldsymbol{\alpha}\, \boldsymbol{\mathcal{P}}(\boldsymbol{\alpha}) \Psi_{\boldsymbol{\alpha}}^*(\mathbf{R}_1, 0) \Psi_{\boldsymbol{\alpha}}(\mathbf{R}_2, 0). \tag{3}$$

Here we use the notation $\mathbf{R} \equiv (X, Y)$ to represent a dimensionless radius vector with $X = x/\sigma_I$, $Y = y/\sigma_I$, and σ_I being any characteristic spatial scale in the beam transverse plane. In particular, it is convenient to assume that σ_I coincides with a beam waist at the source plane. Next,

$$\boldsymbol{\mathcal{P}}(\boldsymbol{\alpha}) = \begin{bmatrix} \mathcal{P}_{xx}(\boldsymbol{\alpha}) & \mathcal{P}_{xy}(\boldsymbol{\alpha}) \\ \mathcal{P}_{yx}(\boldsymbol{\alpha}) & \mathcal{P}_{yy}(\boldsymbol{\alpha}) \end{bmatrix}, \tag{4}$$

is a nonnegative matrix that guarantees nonnegative definiteness of the cross-spectral density matrix [45], and $\{\Psi_{\boldsymbol{\alpha}}(\mathbf{R}, 0)\}$ are the complex Gaussian (pseudo) modes. Further, $\mathrm{d}^4\boldsymbol{\alpha} = \Pi_{s=X,Y} \mathrm{dRe}[\boldsymbol{\alpha}_s] \mathrm{dIm}[\boldsymbol{\alpha}_s]$ and $\boldsymbol{\alpha} = (\mathbf{u} + \mathrm{i}\mathbf{v})/\sqrt{2}$, where Re[·] and Im[·] denote the real and imaginary parts, respectively. The pseudo-modes $\{\Psi_{\boldsymbol{\alpha}}(\mathbf{R}, 0)\}$ at the source are given explicitly by the expression

$$\Psi_{\boldsymbol{\alpha}}(\mathbf{R}, 0) = \frac{\mathrm{e}^{-\mathbf{v}^2/2}}{\sqrt{\pi}} \exp\left[-\frac{(\mathbf{R} - \sqrt{2}\boldsymbol{\alpha})^2}{2}\right]. \tag{5}$$

Here we stress that the pseudo-modes are non-orthogonal and normalized such that

$$\int \mathrm{d}^2\mathbf{R}\, \Psi_{\boldsymbol{\alpha}}^*(\mathbf{R}, 0) \Psi_{\boldsymbol{\alpha}}(\mathbf{R}, 0) = 1, \tag{6}$$

and form an over-complete set implying that

$$\int \mathrm{d}^4\boldsymbol{\alpha}\, \Psi_{\boldsymbol{\alpha}}^*(\mathbf{R}_1, 0) \Psi_{\boldsymbol{\alpha}}(\mathbf{R}_2, 0) = \delta(\mathbf{R}_1 - \mathbf{R}_2), \tag{7}$$

where $\delta(\mathbf{R}_1 - \mathbf{R}_2)$ is a Dirac delta function.

It follows from Eqs. (3)–(7) that the cross-spectral density of **any** partially coherent vector source can be represented by Eq. (3). In addition, the generalized CGR can be applied to synthesize novel partially coherent vector beams via engineering the nonnegative matrix $\boldsymbol{\mathcal{P}}(\boldsymbol{\alpha})$. Moreover, partially coherent vector beam propagation in linear optical media can be simply treated since only Gaussian pseudo-modes, but not the distribution function $\boldsymbol{\mathcal{P}}(\boldsymbol{\alpha})$, are affected by beam propagation.

2.2. Propagation in the optical ABCD system

The cross-spectral density of a partially coherent vector beam field propagating though an ABCD optical system can be expressed at any output plane as

$$\mathbf{W}(\mathbf{R}_1, \mathbf{R}_2, Z) = \int \mathrm{d}^4\boldsymbol{\alpha}\, \boldsymbol{\mathcal{P}}(\boldsymbol{\alpha}) \Psi_{\boldsymbol{\alpha}}^*(\mathbf{R}_1, Z) \Psi_{\boldsymbol{\alpha}}(\mathbf{R}_2, Z), \tag{8}$$

Optics EXPRESS

where

$$\Psi_{\boldsymbol{\alpha}}(\mathbf{R}, Z) = \frac{\sigma_I^2}{\lambda|B|}\int \mathrm{d}^2\mathbf{R}'\Psi_{\boldsymbol{\alpha}}(\mathbf{R}', 0)\mathrm{e}^{\frac{\mathrm{i}k\sigma_I^2}{2B}(A\mathbf{R}'^2 - 2\mathbf{R}\cdot\mathbf{R}' + D\mathbf{R}^2)} \tag{9}$$

is a complex Gaussian pseudo-mode at the output plane; A, B, C, and D are four elements of the transfer matrix of the optical system, and $k = 2\pi/\lambda$ denotes the wavenumber, λ being the wavelength. On substituting from Eq. (5) into Eq. (9), we can obtain an analytical expression for each mode field in any transverse plane $Z \geq 0$ as

$$\Psi_{\boldsymbol{\alpha}}(\mathbf{R}, Z) = \frac{\mathrm{e}^{-\mathbf{v}^2/2}}{\sqrt{\pi}}\frac{\mathrm{i}B}{Z_{AB}|B|}\exp\left\{-\frac{1}{2Z_{AB}}\left[2A\boldsymbol{\alpha}^2 - 2\sqrt{2}\boldsymbol{\alpha}\mathbf{R} + \frac{Z_{AB}D - 1}{\mathrm{i}Z}\mathbf{R}^2\right]\right\}, \tag{10}$$

where $Z = B/z_R$ and $Z_{AB} = A + \mathrm{i}Z$. Here $z_R = k\sigma_I^2$ denotes the Rayleigh range. Using Eq. (9) and a given $\mathcal{P}$-distribution, $\mathcal{P}(\boldsymbol{\alpha})$ in Eq. (8), we can easily obtain the cross-spectral density matrix at the output plane.

3. Self-steering partially coherent vector beams

Consider now a shifted $\mathcal{P}$-distribution such that

$$\mathcal{P}^{(\mathrm{s})}(\boldsymbol{\alpha}) = \mathcal{P}(\boldsymbol{\alpha} - \boldsymbol{\alpha}_0), \tag{11}$$

where $\boldsymbol{\alpha}_0 = (\mathbf{u}_0 + \mathrm{i}\mathbf{v}_0)/\sqrt{2}$. On substituting from Eq. (11) into Eq. (3), we obtain the cross-spectral density matrix of a self-steering partially coherent vector beam field in the source plane in the form

$$\mathbf{W}^{(\mathrm{s})}(\mathbf{R}_1, \mathbf{R}_2, 0) = \mathbf{W}(\mathbf{R}_1 - \mathbf{u}_0, \mathbf{R}_2 - \mathbf{u}_0, 0)\mathrm{e}^{-\mathrm{i}(\mathbf{R}_1 - \mathbf{R}_2)\cdot\mathbf{v}_0}, \tag{12}$$

which clearly shows that the shift variables $\mathbf{u}_0$ and $\mathbf{v}_0$ lead to a spatial displacement and a phase shift of the cross-spectral density matrix at the source.

Next, on substituting from Eq. (11) into Eq. (8), we obtain the cross-spectral density matrix of the self-steering partially coherent vector beam in the output plane of an ABCD optical system as

$$\mathbf{W}^{(\mathrm{s})}(\mathbf{R}_1, \mathbf{R}_2, Z) = \mathbf{W}(\mathbf{R}_1 - \mathbf{D}_0, \mathbf{R}_2 - \mathbf{D}_0, Z)\mathrm{e}^{-\mathrm{i}(\mathbf{R}_1 - \mathbf{R}_2)\cdot\mathbf{P}_0}, \tag{13}$$

where the spatial displacement and the phase shift in the output plane, respectively, can be expressed as

$$\mathbf{D}_0 = A\mathbf{u}_0 + Z\mathbf{v}_0, \tag{14}$$

$$\mathbf{P}_0 = \frac{AD - 1}{Z}\mathbf{u}_0 + D\mathbf{v}_0. \tag{15}$$

For free space beam propagation $A = 1, B = z, C = 0$, and $D = 1$, and the spatial displacement and phase shift expressions reduce to

$$\mathbf{D}_0 = \mathbf{u}_0 + Z\mathbf{v}_0, \tag{16}$$

$$\mathbf{P}_0 = \mathbf{v}_0, \tag{17}$$

where $Z = z/z_R$ represents a dimensionless propagation distance in free space. Comparing the spatial displacement and phase shift in Eqs. (16) and (17) in the output plane with those in Eq. (12) in the source plane, we find that the spatial displacement of the self-steering partially coherent vector beam on propagation in free space increases with the propagation distance Z at a

Optics EXPRESS

rate determined by the initial phase shift $\mathbf{v}_0$. Moreover, the phase shift $\mathbf{P}_0$ of the beam during propagation in free space remains unchanged.

To gain insight into the evolution properties of the spectral density (intensity) and the polarization state of the self-steering partially coherent vector beam on propagation, we adopt the Stokes parameters [44]

$$S_j(\mathbf{R}, Z) = \mathrm{tr}[\mathbf{\Phi}(\mathbf{R}, Z)\boldsymbol{\sigma}_j], \quad j \in (0, ..., 3), \tag{18}$$

where $\mathbf{\Phi}(\mathbf{R}, Z) = \mathbf{W}(\mathbf{R}, \mathbf{R}, Z)$ denotes a polarization matrix, $\boldsymbol{\sigma}_0$ is the 2×2 unit matrix, and $\boldsymbol{\sigma}_1, \boldsymbol{\sigma}_2, \boldsymbol{\sigma}_3$ are the three Pauli matrices. In the Stokes representation, $S_0(\mathbf{R}, Z)$ is the intensity of the beam, while $S_1(\mathbf{R}, Z)$, $S_2(\mathbf{R}, Z)$, and $S_3(\mathbf{R}, Z)$ determine the fully polarized part of the beam state of polarization. Eqs. (13) and (18) yield the Stokes parameters of the self-steering partially coherent vector beam on propagation

$$S_j^{(s)}(\mathbf{R}, Z) = S_j(\mathbf{R} - \mathbf{D}_0, Z), \quad j \in (0, ..., 3), \tag{19}$$

where the spatial displacement $\mathbf{D}_0$ is expressed by Eq. (14) for a general ABCD optical system and by Eq. (16) for free space. Eq. (19) indicates that not only the intensity but also the polarization state of the self-steering partially coherent vector beam possess a dynamic guiding center on beam propagation. Further, the displacement of the guiding center in free space grows linearly with the propagation distance at the rate $\mathbf{v}_0$. The property of the self-steering partially coherent vector beams can be used for trapped particles transport and mobile targets tracing.

4. Example

As a particular example, we introduce the cylindrically correlated partially coherent (CCPC) vector beams in this section by using the generalized CGR. We then examine the CCPC vector beam and self-steering CCPC vector beam propagation properties both theoretically and experimentally.

4.1. Cylindrically correlated partially coherent vector beams: theory

The $\mathcal{P}$-matrix for an CCPC vector beam source has the form,

$$\mathcal{P}(\boldsymbol{\alpha}) = \delta(\mathbf{u}) \exp(-\frac{\xi_c^2 \mathbf{v}^2}{2}) \begin{bmatrix} a^2(\mathbf{v}) & a(\mathbf{v})b(\mathbf{v}) \\ a(\mathbf{v})b(\mathbf{v}) & b^2(\mathbf{v}) \end{bmatrix}, \tag{20}$$

where $\xi_c = \sigma_c/\sigma_I$ stands for a relative coherence length; σ_c being the coherence length of the CCPC vector beam at the source, and

$$\begin{bmatrix} a(\mathbf{v}) \\ b(\mathbf{v}) \end{bmatrix} = \mathbf{M}(\theta) \begin{bmatrix} v_x \\ v_y \end{bmatrix}, \tag{21}$$

with $\mathbf{M}(\theta)$ being a clockwise rotation matrix and $0 \le \theta < 2\pi$. On substituting from Eqs. (20), (21), and (5) into Eq. (3), we obtain an explicit expression for the CCPC beam cross-spectral density matrix in source plane, as given by Eqs. (39)–(44) of the Appendix. Next, on combining Eqs. (20), (21), and (10) in Eq. (8), we obtain an expression for the cross-spectral density matrix of an CCPC beam transmitted through an ABCD optical system as shown by Eqs. (45)–(52) of the Appendix. In the free space propagation case, the CCPC beam Stokes parameters can then be

expressed as

$$S_0(\mathbf{R}, Z) = 2C_0 \exp\left(-\frac{\mathbf{R}^2}{S_0^2}\right)\left(\frac{1}{S_0^2} - \frac{2Z^2}{\xi_c^2 S_0^4} + \frac{2Z^2\mathbf{R}^2}{\xi_c^2 S_0^6}\right), \tag{22}$$

$$S_1(\mathbf{R}, Z) = \frac{4C_0 Z^2}{\xi_c^2 S_0^6} \exp\left(-\frac{\mathbf{R}^2}{S_0^2}\right)(X^2\cos 2\theta - Y^2\cos 2\theta + 2XY\sin 2\theta), \tag{23}$$

$$S_2(\mathbf{R}, Z) = \frac{4C_0 Z^2}{\xi_c^2 S_0^6} \exp\left(-\frac{\mathbf{R}^2}{S_0^2}\right)(-X^2\sin 2\theta + Y^2\sin 2\theta + 2XY\cos 2\theta), \tag{24}$$

$$S_3(\mathbf{R}, Z) = 0. \tag{25}$$

It is found from Eq. (22) that the CCPC beam intensity is independent of θ. The intensity of a partially coherent and partially polarized vector beam can be viewed as a sum of the polarized part and unpolarized part intensities [44], e.g.,

$$S_0(\mathbf{R}, Z) = S_{0_p}(\mathbf{R}, Z) + S_{0_u}(\mathbf{R}, Z), \tag{26}$$

where $S_{0_p}(\mathbf{R}, Z)$ and $S_{0_u}(\mathbf{R}, Z)$ are intensities of the polarized part and unpolarized part, respectively. The degree of polarization in the spatial-frequency domain is defined by the intensity ratio between the polarized part and the total field [44], i.e.,

$$P(\mathbf{R}, Z) = \frac{S_{0_p}(\mathbf{R}, Z)}{S_0(\mathbf{R}, Z)}, \tag{27}$$

where $S_{0_p}(\mathbf{R}, Z)$ can be obtained from $S_1(\mathbf{R}, Z)$, $S_2(\mathbf{R}, Z)$, $S_3(\mathbf{R}, Z)$ as

$$S_{0_p}(\mathbf{R}, Z) = \sqrt{S_1^2(\mathbf{R}, Z) + S_2^2(\mathbf{R}, Z) + S_3^2(\mathbf{R}, Z)}. \tag{28}$$

We stress here that the Stokes parameters can be measured in experiment by using the combination of the wave plates and polarizers [54]. Thus, the intensities for the polarized and unpolarized parts of the beam can be deduced from the Stokes parameters measurement, although, to the best of our knowledge, in general, one cannot physically separate the polarized and unpolarized parts of the beam [55–58]. Eqs.(22)–(28) yield

$$S_{0_p}(\mathbf{R}, Z) = \frac{4C_0 Z^2\mathbf{R}^2}{\xi_c^2 S_0^6} \exp\left(-\frac{\mathbf{R}^2}{S_0^2}\right), \tag{29}$$

$$S_{0_u}(\mathbf{R}, Z) = \frac{2C_0(\xi_c^2 S_0^2 - 2Z^2)}{\xi_c^2 S_0^4} \exp\left(-\frac{\mathbf{R}^2}{S_0^2}\right), \tag{30}$$

and

$$P(\mathbf{R}, Z) = \frac{2Z^2\mathbf{R}^2}{\xi_c^2 S_0^4 - 2Z^2 S_0^2 + 2Z^2\mathbf{R}^2}. \tag{31}$$

It can be inferred from Eqs. (29) and (30) that the polarized part intensity vanishes in the source plane (i.e., $S_{0_p}(\mathbf{R}, 0) = 0$). This implies that **any** CCPC vector beam in the source plane is completely unpolarized. This conclusion can also be obtained by taking $Z = 0$ into Eq. (31) (i.e., $P(\mathbf{R}, Z = 0) = 0$). Further, we find that for the polarized part, the intensity always displays a doughnut shape with a dark notch at the center, i.e., the intensity for the polarized part at center $S_{0_p}(\mathbf{R} = 0, Z) = 0$, on CCPC vector beam propagation. Thus, the field at center ($\mathbf{R} = 0$) remains unpolarized during propagation, i.e., the degree of polarization at center $P(\mathbf{R} = 0, Z) = 0$. By

Optics EXPRESS

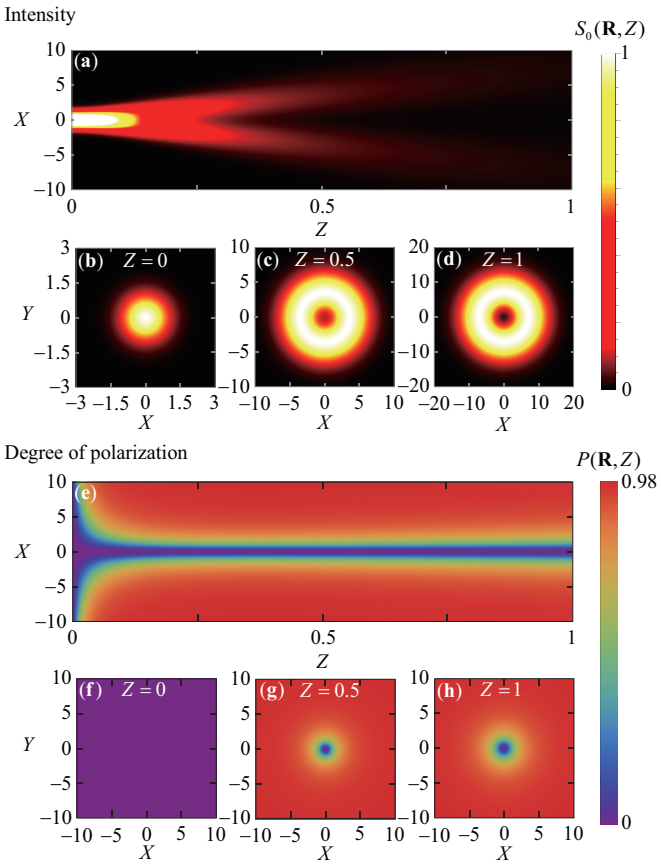

Fig. 1. Calculated intensity distribution $S_0(\mathbf{R}, Z)$ and degree of polarization $P(\mathbf{R}, Z)$ of a CCPC vector beam propagating in free space. (a) The intensity distribution in the $X-Z$ plane ($Y=0$); (b), (c), and (d) The intensity distribution in the $X-Y$ plane at propagation distances $Z=0$, $Z=0.5$, and $Z=1$, respectively; (e) The distribution of the degree of polarization in the $X-Z$ plane ($Y=0$); (f), (g), and (h) The distribution of the degree of polarization in the $X-Y$ plane at propagation distances $Z=0$, $Z=0.5$, and $Z=1$, respectively. The effective coherence length of the CCPC vector beam is $\xi_c=0.2$ and the normalization factor is $C_0=1$. The displayed intensities are normalized with respect to their maximum values.

the same token, the unpolarized part intensity remains Gaussian throughout beam propagation as shown in Eq. (30). Further, Eqs. (29) and (30) show that the polarized part intensity monotonically increases with Z, while the unpolarized part intensity monotonically decreases. This implies that the generated CCPC beam becomes progressively more polarized on propagation and its dark hollow core grows in size.

The above predictions are illustrated in Fig. 1 in which we display the intensity distribution and the degree of polarization of a CCPC vector beam propagating in the free space. Figure 1 reveals that the CCPC vector beam in the source plane is unpolarized and has a Gaussian profile. Figures 1(a)–(d) shows that the intensity distribution in free space indeed transforms from an initial Gaussian to a doughnut shape with the increase of the propagation distance. This is due to

Optics EXPRESS

the increase of the polarization of the beam as shown in Figs. 1(e)–(h). Further, it is noted in Fig. 1(e) that the degree of polarization keeps zero at the beam center ($\mathbf{R} = 0$) during propagation.

Next, we examine the polarization state of the CCPC vector beam. The polarized part of the CCPC beam polarization state is encapsulated in the three Stokes parameters: $S_1(\mathbf{R}, Z)$, $S_2(\mathbf{R}, Z)$, and $S_3(\mathbf{R}, Z)$. For a CCPC vector beam, we have $S_3(\mathbf{R}, Z) = 0$, implying that the fully polarized part has linear polarization. Moreover, the ratio of $S_1(\mathbf{R}, Z)$ to $S_2(\mathbf{R}, Z)$ can be written as

$$\frac{S_1(\mathbf{R}, Z)}{S_2(\mathbf{R}, Z)} = \frac{X^2 \cos 2\theta - Y^2 \cos 2\theta + 2XY \sin 2\theta}{-X^2 \sin 2\theta + Y^2 \sin 2\theta + 2XY \cos 2\theta}, \tag{32}$$

indicating that the fully polarized part of the CCPC vector beam displays cylindrical polarization [59]. The polarization state distribution is controlled by the angle θ. For examples, for $\theta = 0$, the ratio in Eq. (32) reduces to $(X^2 - Y^2)/(2XY)$ indicating a radial polarization distribution. While, for $\theta = \pi/2$, the ratio reduces to $(-X^2 + Y^2)/(-2XY)$ indicating an azimuthal polarization distribution. Instead of a radial polarization or azimuthal polarization, in general, each point of the beam has a polarization rotated by θ from its radial direction. Such polarization state distribution is the generalized cylindrical polarization distribution [59]. Further, it is found in Eq. (32) that the ratio is independent of the propagation distance Z, which indicates that the state of polarization for the CCPC vector beam remains invariant on propagation (except for the unpolarized beam source). In Fig. 2 we display the CCPC beam polarization distribution at the distance $Z = 1$ for different values of θ. We find that the beam is radially polarized for $\theta = 0$ and becomes azimuthally polarized for $\theta = \pi/2$, while for $\theta = \pm\pi/4$ the CCPC vector beam shows the generalized cylindrical polarization distribution.

The degree of polarization for the beam at a certain plane on propagating depends on the transverse position $\mathbf{R}$. To examine the global polarization (akin to the global degree of coherence), we introduce a polarization purity, which is defined as fraction of the beam energy carried by the polarized part, i.e.,

$$\eta_p(Z) = \frac{\int \mathrm{d}^2\mathbf{R}\, S_{0_p}(\mathbf{R}, Z)}{\int \mathrm{d}^2\mathbf{R}\, S_0(\mathbf{R}, Z)}. \tag{33}$$

This real-valued quantity is independent of the transverse position $\mathbf{R}$ and bounded as $0 \le \eta_p(Z) \le 1$, with the upper and lower limits corresponding to a fully polarized and completely unpolarized beam, respectively, whereas the intermediate values representing partially polarized beams.

In Fig. 3, we display the polarization purity $\eta_p(Z)$ of a CCPC vector beam propagating in free space as a function of the effective coherence length ξ_c and propagation distance Z. We observe in Fig. 3 that the polarization purity is zero in the source plane ($Z = 0$), which implies that the CCPC vector beam source is completely unpolarized. The polarization purity increases, though, with the propagation distance Z. We also see that the source effective coherence length strongly

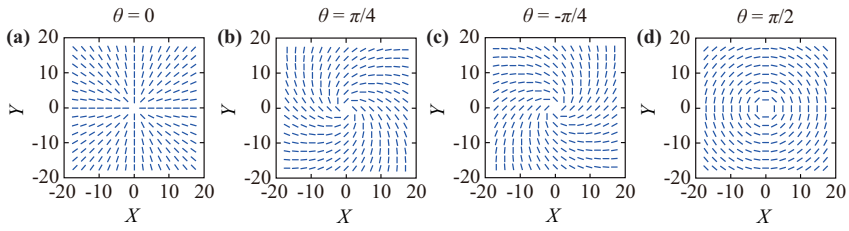

Fig. 2. Distribution of the CCPC vector beam polarization states at the distance $Z = 1$ with (a) $\theta = 0$; (b) $\theta = \pi/4$; (c) $\theta = -\pi/4$; (d) $\theta = \pi/2$. The effective spatial coherence length at the source is $\xi_c = 0.2$ and the normalization factor is $C_0 = 1$. The blue lines in the figure denote linear polarization states.

Optics EXPRESS

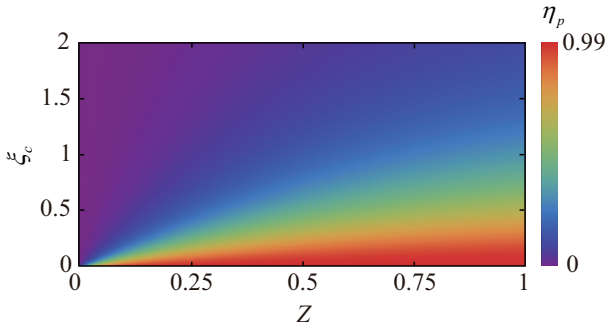

Fig. 3. Polarization purity $\eta_p(Z)$ for a CCPC vector beam propagating in free space as a function of the effective coherence length ξ_c at the source and propagation distance Z.

affects the polarization purity: the latter increases as the former decreases on propagation. In particular, at $Z = 1$ (Rayleigh range), the polarization purity is nearly zero for large magnitudes of ξ_c, yet it is close to 99% for $0 < \xi_c \leq 0.4$. Thus, a very pure polarization state (with 99% polarization purity) can be attained by a CCPC vector beam with low initial spatial coherence.

4.2. *Cylindrically correlated partially coherent vector beams: experiment*

We now report experimental realization of CCPC vector beams. The schematic of our experimental setup is shown in Fig. 4, which is similar to those reported in [46]. In our experiment, we first generate a spatially incoherent, cylindrically polarized vector beam by using a polarization converter [59–61] and a rotating ground-glass disk. The following shows the experiment details. A linearly polarized beam emitted from a monochromatic He-Ne laser of wavelength 633 nm passes through a beam expander (BE) and neutral density filter (NDF) and reflected by a reflecting mirror, then it goes towards a linear polarizer (LP) and a radial-polarization converter (RPC) (ARCoptix) (the photograph is shown in the inset (a) of Fig. 4). The RPC is a liquid crystal device that can convert a conventional linearly polarized beam into a beam that has a stable radial or azimuthal polarization distribution. In our experiment, a radially polarized beam with vectorial electric field $\mathbf{E}(\mathbf{v}) = E_0(\mathbf{v})\hat{\mathbf{e}}_r$ is generated from the RPC, where $E_0(\mathbf{v})$ is the amplitude of the field and $\hat{\mathbf{e}}_r$ is the unit vector in the radial direction. To generate the generalized cylindrically polarized beam, we apply the double half-wave plates (HWPs) system [60, 61] as shown in the inset (b) of Fig. 4. By rotating the second HWP, we let angle between the fast axes of two half-wave plates be φ. The Jones matrix of the system then can be written as [60]

$$\mathbf{J}(\varphi) = \begin{bmatrix} \cos(2\varphi) & -\sin(2\varphi) \\ \sin(2\varphi) & \cos(2\varphi) \end{bmatrix}. \tag{34}$$

Thus, the electric field of the beam from double HWPs system can be obtained as

$$\mathbf{E}(\mathbf{v}) = E_0(\mathbf{v})[\cos\theta\hat{\mathbf{e}}_r + \sin\theta\hat{\mathbf{e}}_\phi], \tag{35}$$

where $\hat{\mathbf{e}}_\phi$ denotes the unit vector in the azimuthal direction, and $\theta = 2\varphi$ represent the polarization rotation angle of each point of the beam from its radial direction. By simply rotating the second HWP, we can vary θ, thus generating different cylindrically polarized beam. After passing through a thin lens L1 with focal length $f_1 = 150$ mm, the generated cylindrically polarized beam illuminates a rotating ground-glass disk (RGGD), producing a spatially incoherent cylindrically polarized beam. A step-by-step guide to reduce the spatial coherence of laser light using a RGGD

Optics EXPRESS

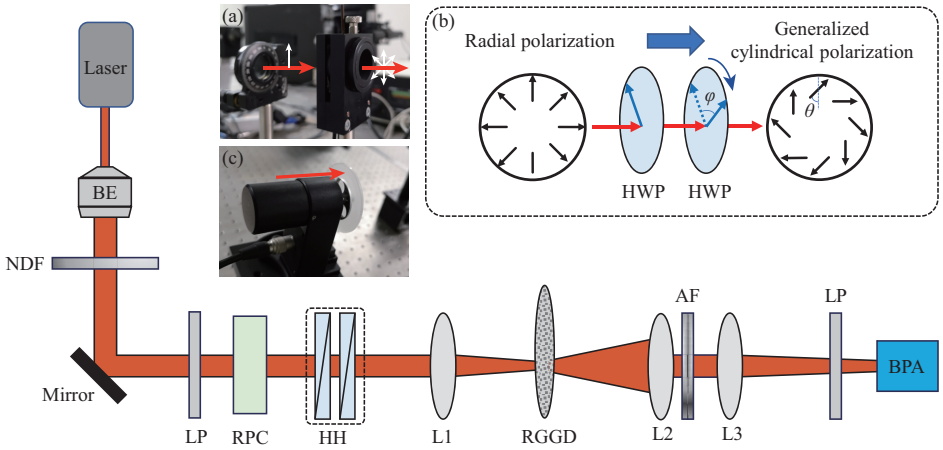

Fig. 4. Schematic of the experimental setup for generating and measuring the cylindrically correlated partially coherent vector beam. The laser source used in our experiment is a monochromatic He-Ne laser of wavelength being 633 nm. BE: beam expander; NDF: neutral density filter; LP: linear polarizer; RPC: radial-polarization converter; HH: double half-wave plates (HWPs) system as shown in the inset (b); L1, L2, L3: thin lenses; RGGD: rotating ground-glass disk; AF: Gaussian amplitude filter; BPA: beam profile analyzer. Inset (a): photograph of the LP (left) and RPC (right) that can convert a linearly polarized beam into a radially polarized beam. Inset (b): converting a radially polarized beam to a generalized cylindrically polarized beam by a double half-wave plates system. As shown in the inset φ is the angle between the fast axes of the two HWPs, while θ is the clockwise rotation angle of the linear polarization in the generalized cylindrical polarization distribution with respect to that in the radial polarization distribution. Here the relation between θ and φ is given by $\theta = 2\varphi$. Inset (c): photograph of the RGGD that is driven by the controller of a optical chopper system.

can be found in [62]. The photograph of RGGD used in our experiment is shown in the inset (c) of Fig. 4. The surface roughness of ground-glass disk used in our experiment is 400 mesh number and the rotating speed is 3000 r/min that is controlled by the controller of a optical chopper system (MC2000B, THORLABS). We stress that the transmitted beam from the RGGD can be regarded as an incoherent cylindrically polarized beam if the diameter of the beam spot on the RGGD is larger than the inhomogeneity scale of RGGD [63, 64], and this condition is satisfied in our experiment.

The polarization matrix describing the incoherent cylindrically polarized beam is $\mathbf{\Phi}(\mathbf{v}) = \boldsymbol{\mathcal{P}}(\boldsymbol{\alpha})/\delta(\mathbf{u})$, where $\boldsymbol{\mathcal{P}}(\boldsymbol{\alpha})$ is given by Eqs. (20) and (21). After the incoherent cylindrically polarized vector beam has passed through a thin lens L2 and a Gaussian amplitude filter (AF), the cross-spectral density matrix of the output beam can be expressed by [46]

$$\mathbf{W}(\mathbf{r}_1, \mathbf{r}_2, \omega) = \int \mathbf{\Phi}(\mathbf{v}) H^*(\mathbf{r}_1, \mathbf{v}) H(\mathbf{r}_2, \mathbf{v}) \mathrm{d}^2\mathbf{v}, \tag{36}$$

where

$$H(\mathbf{r}, \mathbf{v}) = \frac{-\mathrm{i}}{\lambda f_2} T(\mathbf{r}) \exp[\frac{\mathrm{i}\pi}{\lambda f_2}(\mathbf{v}^2 - 2\mathbf{r}\cdot\mathbf{v})] \tag{37}$$

is the response function of the optical system between the incoherent source and the output field, $f_2 = 250$ mm is the focal length of L2, and $T(\mathbf{r}) = \exp(-\mathbf{r}^2/4\sigma_I^2)$ denotes the transmission function of AF with σ_I being the beam width. Taking the polarization matrix $\mathbf{\Phi}(\mathbf{v})$ for the

Optics EXPRESS

incoherent cylindrically polarized beam and $H(\mathbf{r}, \mathbf{v})$ in Eq. (37) into Eq. (36), we obtain that the cross-spectral density matrix for the output beam has the same form as that for the CCPC vector beam (i.e., Eqs. (39)–(44)). Thus, the output field from AF is the CCPC vector source. The transverse coherence length of the CCPC source can be expressed as $\sigma_c = \lambda f_2/(\pi\omega_0)$, where ω_0 is the beam width of the spot on the RGGD. The beam width of the spot on the RGGD (and thus the transverse coherence length) can be simply controlled by varying the distance between L1 and RGGD. The transverse coherence length and the beam width of the CCPC source in our experiment are $\sigma_c = 0.2$ mm and $\sigma_I = 1$ mm, respectively. To efficiently measure the beam intensity during propagation, we focus the beam by a thin lens with the focal length $f_3 = 400$ mm, and measure the intensity of the focused CCPC vector beam by using a beam profile analyzer (BPA). Figure 5 displays the experimental results for the intensity distribution of the focused CCPC vector beam at several propagation distances. We find that the CCPC beam has a Gaussian intensity profile at the source, but gradually becomes doughnut shaped on propagation, as we have predicted above.

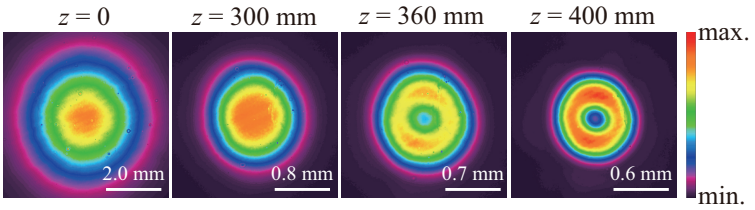

Fig. 5. Experimental intensity distribution of a CCPC vector beam transmitted through a thin lens with the focal distance $f_3 = 400$ mm at several propagation distances. The source transverse coherence length and beam width are $\sigma_c = 0.2$ mm and $\sigma_I = 1$ mm, respectively. The beam wavelength is 633 nm.

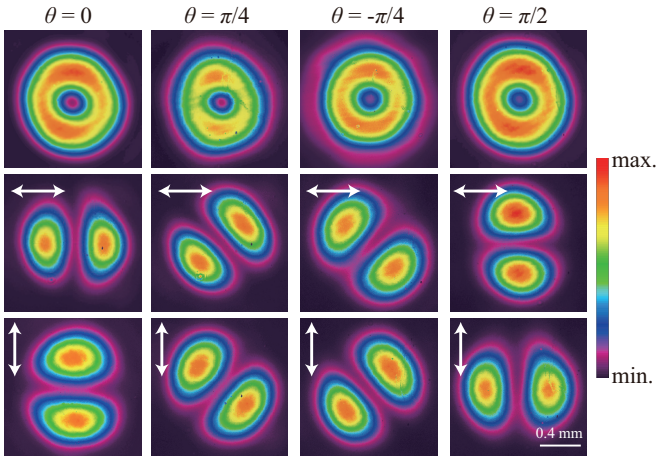

Fig. 6. Experimental results for the total intensities (top panel), the x-polarized (middle panel), and y-polarized (bottom panel) component intensities of CCPC vector beams with four different polarization distributions in the focal plane. The focal distance of the lens is 400 mm. The source coherence length and beam width are 0.2 mm and 1 mm, respectively. The beam wavelength is 633 nm. The white arrows in the figure denote the transmission direction of the linear polarizer.

To check the polarization state of the generated CCPC vector beam, we insert a linear polarizer with the transmission angle of either 0° or 90° with respect to the x-axis into the beam path and measure the intensity of the x-polarized and y-polarized components in the focal plane of the lens. Figure 6 displays experimental results for the total intensities (top panel), x-polarized (middle panel), and y-polarized (bottom panel) components of the beam with four different polarization distributions in the focal plane. The left panel of Fig. 6 reveals that the CCPC beam displays radial polarization in the focal plane when the angle between the fast axes of the two HWPs is fixed at $\varphi = 0$ (now $\theta = 0$, see Fig. 2(d) for the polarization distribution). The right panel reveals that the beam exhibits azimuthal polarization when $\varphi = \pi/4$ (now $\theta = \pi/2$, see Fig. 2(d) for the polarization distribution). The polarization states in the second column and third column of Fig. 6 correspond to the polarization distributions in Figs. 2(b) and 2(c).

4.3. *Self-steering cylindrically correlated partially coherent vector beams*

As we have discussed in Sec. 3, by adding a spatial displacement in the $\mathcal{P}(\boldsymbol{\alpha})$-matrix, a phase shift will appear in the cross-spectral density matrix of the self-steering vector beam source. Not only the intensity but also the polarization state of such vector beam possess a dynamic guiding center on beam propagation due to the phase shift in the source plane. Further, during propagation, the beam shape and polarization distribution will keep practically invariant. Next, we will study the experimental generation of self-steering CCPC vector beam, and verify its steering propagation properties. To this end, we first introduce a spatial displacement $\boldsymbol{\rho}_0$ in the polarization matrix of the incoherent cylindrically polarized beam through using an off-axis cylindrically polarized beam to illuminate the RGGD. The schematic of the experimental setup is shown in Fig. 7. Taking the shifted polarization matrix $\boldsymbol{\Phi}(\mathbf{v} - \boldsymbol{\rho}_0)$ into Eq. (36), we obtain that the cross-spectral density matrix of the output field can be expressed by Eq. (12), in which the spatial displacement $\mathbf{u}_0 = 0$ and the phase shift

$$\mathbf{v}_0 = 2\pi\sigma_I\boldsymbol{\rho}_0/(\lambda f_2). \tag{38}$$

This way, the self-steering CCPC vector source is generated experimentally. It is found from Eq. (38) that the parameter $\mathbf{v}_0$ of the source can be simply controlled by varying the displacement $\boldsymbol{\rho}_0$ of the off-axis cylindrically polarized beam.

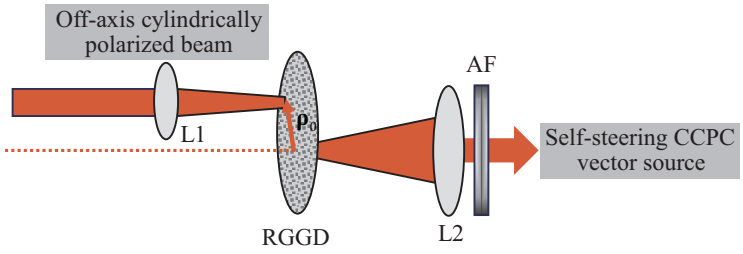

Fig. 7. Schematic of the experimental setup for generating the self-steering CCPC vector source from a focused off-axis cylindrically polarized beam. Here $\boldsymbol{\rho}_0$ is the off-axis displacement of the cylindrically polarized beam on the rotating ground-glass disk (RGGD). L and AF in the figure denote the thin lenses and Gaussian amplitude filter, respectively.

We now study experimentally the propagation properties of the focused self-steering CCPC beam, and measure the intensity and polarization state (through x and y polarized components of the intensity) during propagation. The focal distance of the lens used in our experiment is 400 mm. The distance between the self-steering CCPC source and the BPA is equal to z. In

Optics EXPRESS

Fig. 8, we display the experimental results for the total intensity (top panel), x-polarized (middle panel), and y-polarized (bottom) components of intensity of a focused self-steering CCPC vector beam with the initial phase shift $\mathbf{v}_0 = (10, 10)$ at different propagation distances. The angle between the fast axes of the two HWPs is set to be $\varphi = 0$. Thus, the polarization of the beam during propagation has a radial polarization distribution. We can infer from Fig. 8 that the focused self-steering CCPC vector beam propagates with a mobile steering centre. We note also that the corresponding polarization state behavior can be inferred from that of the intensity components and it is in agreement with our theoretical prediction. We would stress here that although the apparent beam focusing in the figure is caused by the lens, the lens is not essential for beam self-steering [32].

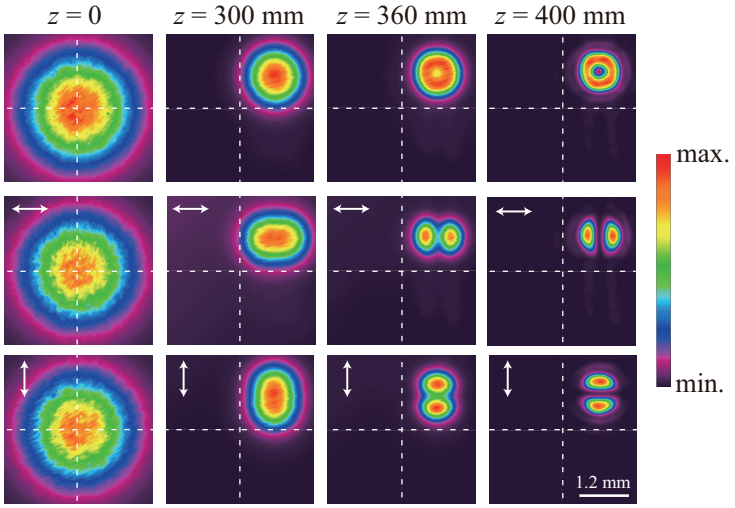

Fig. 8. Experimental results for the total intensity (top panel), the x-polarized (middle panel), and y-polarized (bottom panel) component intensities of a self-steering CCPC vector beam transmitted through a thin lens with focal distance $f = 400$ mm at several propagation distances. The source coherence and beam width are 0.2 mm and 1 mm, respectively. The phase shift for the source is $\mathbf{v}_0 = (10, 10)$. The beam wavelength is 633 nm. The white arrows in the figure denote the transmission direction of the linear polarizer.

5. Conclusions

In this work, we have introduced partially coherent vector beams with mobile guiding centers of their intensity and polarization states, referred to as the self-steering partially coherent vector beams. As a particular example, we proposed the concept of cylindrically correlated partially coherent (CCPC) vector beams and studied their free space propagation properties. The CCPC beams become progressively more polarized on propagation and they acquire doughnut shape profiles. Further, we found that very pure far-field cylindrical polarization states (with 99% polarization purity) can be created by the CCPC sources of low spatial coherence. We have also experimentally generated CCPC vector beams with different cylindrical polarization states. Further, the self-steering CCPC vector beam with tailored directivity of both intensity and polarization state has been generated and measured in our experiment. The vectorial self-steering effect of optical beam can be used for polarization array generation [65], e.g., via a superposition of uncorrelated self-steering vector beams with different guiding centers. Such polarization

Optics EXPRESS

arrays can be useful for particle sorting and multiple surface wave excitation.

Appendix

The cross-spectral density matrix for the CCPC vector beam in the source plane reads

$$W_{xx}(\mathbf{R}_1, \mathbf{R}_2, 0) = C_0 \left[1 - \frac{1}{\xi_c^2} a^2(|\mathbf{R}_1 - \mathbf{R}_2|)\right] \exp\left[-\frac{(\mathbf{R}_1 - \mathbf{R}_2)^2}{2\xi_c^2}\right] \exp\left(-\frac{\mathbf{R}_1^2 + \mathbf{R}_2^2}{2}\right), \tag{39}$$

$$W_{yy}(\mathbf{R}_1, \mathbf{R}_2, 0) = C_0 \left[1 - \frac{1}{\xi_c^2} b^2(|\mathbf{R}_1 - \mathbf{R}_2|)\right] \exp\left[-\frac{(\mathbf{R}_1 - \mathbf{R}_2)^2}{2\xi_c^2}\right] \exp\left(-\frac{\mathbf{R}_1^2 + \mathbf{R}_2^2}{2}\right), \tag{40}$$

$$W_{xy}(\mathbf{R}_1, \mathbf{R}_2, 0) = -C_0 \frac{1}{\xi_c^2} a(|\mathbf{R}_1 - \mathbf{R}_2|) b(|\mathbf{R}_1 - \mathbf{R}_2|) \exp\left[-\frac{(\mathbf{R}_1 - \mathbf{R}_2)^2}{2\xi_c^2}\right] \exp\left(-\frac{\mathbf{R}_1^2 + \mathbf{R}_2^2}{2}\right), \tag{41}$$

$$W_{yx}(\mathbf{R}_1, \mathbf{R}_2, 0) = W_{xy}^*(\mathbf{R}_2, \mathbf{R}_1, 0), \tag{42}$$

where C_0 is a constant and

$$a(|\mathbf{R}_1 - \mathbf{R}_2|) = |X_1 - X_2| \cos\theta + |Y_1 - Y_2| \sin\theta, \tag{43}$$

$$b(|\mathbf{R}_1 - \mathbf{R}_2|) = -|X_1 - X_2| \sin\theta + |Y_1 - Y_2| \cos\theta. \tag{44}$$

The cross-spectral density matrix for the CCPC vector beam in the output plane of an optical ABCD system is obtained as

$$W_{xx}(\mathbf{R}_1, \mathbf{R}_2, Z) = \frac{C_0}{S_0^2} S(\mathbf{R}_1, \mathbf{R}_2, Z) \left\{1 + \frac{2B^2}{k^2 \sigma_c^2 S_0^2 \sigma_I^2} \left[\frac{\sigma_I^2}{2S_0^2} (T_{xx} \cos\theta + T_{yy} \sin\theta)^2 - 1\right]\right\}, \tag{45}$$

$$W_{yy}(\mathbf{R}_1, \mathbf{R}_2, Z) = \frac{C_0}{S_0^2} S(\mathbf{R}_1, \mathbf{R}_2, Z) \left\{1 + \frac{2B^2}{k^2 \sigma_c^2 S_0^2 \sigma_I^2} \left[\frac{\sigma_I^2}{2S_0^2} (-T_{xx} \sin\theta + T_{yy} \cos\theta)^2 - 1\right]\right\}, \tag{46}$$

$$W_{xy}(\mathbf{R}_1, \mathbf{R}_2, Z) = \frac{C_0 B^2}{S_0^6 k^2 \sigma_c^2} S(\mathbf{R}_1, \mathbf{R}_2, Z) (T_{xx} \cos\theta + T_{yy} \sin\theta)(-T_{xx} \sin\theta + T_{yy} \cos\theta), \tag{47}$$

$$W_{yx}(\mathbf{R}_1, \mathbf{R}_2, Z) = W_{xy}^*(\mathbf{R}_2, \mathbf{R}_1, Z), \tag{48}$$

with

$$S(\mathbf{R}_1, \mathbf{R}_2, Z) = \exp\left[\frac{\mathrm{i}(S_0^2 D - A)}{2Z S_0^2} (\mathbf{R}_2^2 - \mathbf{R}_1^2) - \frac{1}{4S_0^2} (\mathbf{R}_1 + \mathbf{R}_2)^2 - \frac{\xi_c^2 + 2}{4\xi_c^2 S_0^2} (\mathbf{R}_1 - \mathbf{R}_2)^2\right], \tag{49}$$

$$S_0^2 = A^2 + Z^2 + \frac{2Z^2}{\xi_c^2}, \tag{50}$$

$$T_{xx} = \frac{1}{\sigma_I} \left[(X_1 + X_2) + \frac{\mathrm{i}A}{Z} (X_2 - X_1)\right], \tag{51}$$

$$T_{yy} = \frac{1}{\sigma_I} \left[(Y_1 + Y_2) + \frac{\mathrm{i}A}{Z} (Y_2 - Y_1)\right]. \tag{52}$$

Optics EXPRESS

Funding

National Natural Science Foundation of China (NSFC) (11525418, 91750201, 61505046); National Sciences and Engineering Research Council of Canada (RGPIN-2018-05497); Natural Science Foundation of Zhejiang Province of China (LY19A040010, LY19A040011); Natural Science of Shandong Province (ZR2019QA004); Construction Project of Postgraduate Core Course of Hangzhou Dianzi University (HXKC2017019).

References

1. L. Mandel and E. Wolf, *Optical Coherence and Quantum Optics* (Cambridge University, 1995).
2. Y. Cai, Y. Chen, and F. Wang, "Generation and propagation of partially coherent beams with nonconventional correlation functions: a review," J. Opt. Soc. Am. A **31**, 2083–2096 (2014).
3. F. Gori and M. Santarsiero, "Devising genuine spatial correlation functions," Opt. Lett. **32**, 3531–3533 (2007).
4. H. Lajunen and T. Saastamoinen, "Propagation characteristics of partially coherent beams with spatially varying correlations," Opt. Lett. **36**, 4104–4106 (2011).
5. S. Sahin and O. Korotkova, "Light sources generating far fields with tunable flat profiles," Opt. Lett. **37**, 2970–2972 (2012).
6. Y. Chen, J. Gu, F. Wang, and Y. Cai, "Self-splitting properties of a Hermite-Gaussian correlated Schell-model beam," Phys. Rev. A **91**, 013823 (2015).
7. M. Santarsiero, R. Martínez-Herrero, D. Maluenda, J. C. G. de Sande, G. Piquero, and F. Gori, "Partially coherent sources with circular coherence," Opt. Lett. **42**, 1512–1515 (2017).
8. G. Piquero, M. Santarsiero, R. Martínez-Herrero, J. C. G. de Sande, M. Alonzo, and F. Gori, "Partially coherent sources with radial coherence," Opt. Lett. **43**, 2376–2379 (2018).
9. X. Lu, Y. Shao, C. Zhao, S. Konijnenberg, X. Zhu, Y. Tang, Y. Cai, and H. Urbach, "Noniterative spatially partially coherent diffractive imaging using pinhole array mask," Adv. Photon. **1**, 016005 (2019).
10. A. Norrman, T. Setälä, and A. T. Friberg, "Partial spatial coherence and partial polarization in random evanescent fields on lossless interfaces," J. Opt. Soc. Am. A **28**, 391–400 (2011).
11. A. Norrman, S. A. Ponomarenko, and A. T. Friberg, "Partially coherent surface plasmon polaritons," Europhys. Lett. **116**, 64001 (2016).
12. Y. Chen, A. Norrman, S. A. Ponomarenko, and A. T. Friberg, "Plasmon coherence determination by nanoscattering," Opt. Lett. **42**, 3279–3282 (2017).
13. Y. Chen, A. Norrman, S. A. Ponomarenko, and A. T. Friberg, "Partially coherent axiconic surface plasmon polariton fields," Phys. Rev. A **97**, 041801 (2018).
14. Y. Chen, A. Norrman, S. A. Ponomarenko, and A. T. Friberg, "Coherence lattices in surface plasmon polariton fields," Opt. Lett. **43**, 3429–3432 (2018).
15. H. Mao, Y. Chen, S. A. Ponomarenko, and A. T. Friberg, "Coherent pseudo-mode representation of partially coherent surface plasmon polaritons," Opt. Lett. **43**, 1395–1398 (2018).
16. F. Wang, X. Liu, Y. Yuan, and Y. Cai, "Experimental generation of partially coherent beams with different complex degrees of coherence," Opt. Lett. **38**, 1814–1816 (2013).
17. J. Lehtolahti, M. Kuittinen, J. Turunen, and J. Tervo, "Coherence modulation by deterministic rotating diffusers," Opt. Express **23**, 10453-10466 (2015).
18. M. W. Hyde IV, S. R. Bose-Pillai, D. G. Voelz, and X. Xiao, "Generation of vector partially coherent optical sources using phase-only spatial light modulators," Phys. Rev. Appl. **6**, 064030 (2016).
19. M. W. Hyde IV, S. R. Bose-Pillai, and R. A. Wood, "Synthesis of non-uniformly correlated partially coherent sources using a deformable mirror," Appl. Phys. Lett. **111**, 101106 (2017).
20. X. Chen, J. Li, S. M. H. Rafsanjani, and O. Korotkova, "Synthesis of Im-Bessel correlated beams via coherent modes," Opt. Lett. **43**, 3590–3593 (2018).
21. S. Knitter, C. Liu, B. Redding, M. K. Khokha, M. A. Choma, and H. Cao, "Coherence switching of a degenerate VECSEL for multimodality imaging," Optica **3**, 403–406 (2016).
22. H. Lajunen and T. Saastamoinen, "Non-uniformly correlated partially coherent pulses," Opt. Express **21**, 190–195 (2013).
23. C. Ding, O. Korotkova, and L. Z. Pan, "The control of pulse profiles with tunable temporal coherence," Phys. Lett. A **378**, 1687–1690 (2014).
24. C. Ding, M. Koivurova, J. Turunen, T. Setälä, and A. T. Friberg, "Coherence control of pulse trains by spectral phase modulation," J. Opt. **19**, 095501 (2017).
25. C. Ding, M. Koivurova, J. Turunen, and L. Pan, "Temporal self-splitting of optical pulses," Phys. Rev. A **97**, 053838 (2018).
26. C. Nelson, S. Avramov-Zamurovic, O. Korotkova, S. Guth, and R. Malek-Madani, "Scintillation reduction in pseudo Multi-Gaussian Schell Model beams in the maritime environment," Opt. Commun. **364**, 145–149 (2016).
27. S. Avramov-Zamurovic, C. Nelson, S. Guth, and O. Korotkova, "Flatness parameter influence on scintillation reduction for multi-Gaussian Schell-model beams propagating in turbulent air," Appl. Opt. **55**, 3442–3446 (2016).

Optics EXPRESS

28. C. Liang, G. Wu, F. Wang, W. Li, Y. Cai, and S. A. Ponomarenko, "Overcoming the classical Rayleigh diffraction limit by controlling two-point correlations of partially coherent light sources," Opt. Express **25**, 28352–28362 (2017).
29. R. Chriki, S. Mahler, C. Tradonsky, V. Pal, A. A. Friesem, and N. Davidson, "Spatiotemporal supermodes: Rapid reduction of spatial coherence in highly multimode lasers," Phys. Rev. A **98**, 023812 (2018).
30. C. Ping, C. Liang, F. Wang, and Y. Cai, "Radially polarized multi-Gaussian Schell-model beam and its tight focusing properties," Opt. Express **25**, 32475–32490 (2017).
31. L. Ma and S. A. Ponomarenko, "Optical coherence gratings and lattices," Opt. Lett. **39**, 6656–6659 (2014).
32. Y. Chen, S. A. Ponomarenko, and Y. Cai, "Self-steering partially coherent beams," Sci. Rep. **7**, 39957 (2017).
33. F. Gori and M. Santarsiero, "Devising genuine twisted cross-spectral densities," Opt. Lett. **43**, 595–598 (2018).
34. R. Borghi, "Twisting partially coherent light," Opt. Lett. **43**, 1627–1630 (2018).
35. O. Korotkova and X. Chen, "Phase structuring of the complex degree of coherence," Opt. Lett. **43**, 4727–4730 (2018).
36. L. Ma and S. A. Ponomarenko, "Free-space propagation of optical coherence lattices and periodicity reciprocity," Opt. Express **23**, 1848–1856 (2015).
37. C. Brosseau, *Fundamentals of Polarized Light: A Statistical Approach* (Wiley, 1998).
38. D. F. V. James, "Change of polarization of light beams on propagation in free space," J. Opt. Soc. Am. A **11**, 1641–1643 (1994).
39. I. Vidal, E. J. S. Fonseca, and J. M. Hickmann, "Light polarization control during free-space propagation using coherence," Phys. Rev. A **84**, 033836 (2011).
40. F. Gori, "Matrix treatment for partially polarized, partially coherent beams," Opt. Lett. **23**, 241–243 (1998).
41. E. Wolf, "Unified theory of coherence and polarization of random electromagnetic beams," Phys. Lett. A **312**, 263–267 (2003).
42. E. Wolf, *Introduction to the Theory of Coherence and Polarization of Light* (Cambridge University, 2007).
43. Y. Cai, F. Wang, C. Zhao, S. Zhu, G. Wu, and Y. Dong, *Vectorial Optical Fields: Fundamentals and Applications*, Q. Zhen, ed. (World Scientific, 2013), Chap. 7, pp. 221–273.
44. A. T. Friberg and T. Setälä, "Electromagnetic theory of optical coherence," J. Opt. Soc. Am. A **33**, 2431–2442 (2016).
45. F. Gori, V. R. Sanchez, M. Santarsiero, and T. Shirai, "On genuine cross-spectral density matrices," J. Opt. A: Pure Appl. Opt. **11**, 085706 (2009).
46. Y. Chen, F. Wang, L. Liu, C. Zhao, Y. Cai, and O. Korotkova, "Generation and propagation of a partially coherent vector beam with special correlation functions," Phys. Rev. A **89**, 013801 (2014).
47. J. M. Auñón and M. Nieto-Vesperinas, "Partially coherent fluctuating sources that produce the same optical force as a laser beam," Opt. Lett. **38**, 2869–2872 (2013).
48. W. M. Steen and J. Mazumder, *Laser Material Processing* (Springer, 2007).
49. S. A. Ponomarenko, "Complex Gaussian representation of statistical pulses," Opt. Express **19**, 17086–17091 (2011).
50. Y. Chen, S. A. Ponomarenko, and Y. Cai, "Experimental generation of optical coherence lattices," Appl. Phys. Lett. **109**, 061107 (2016).
51. S. A. Ponomarenko, "Self-imaging of partially coherent light in graded-index media," Opt. Lett. **40**, 566–568 (2015).
52. X. Liu, J. Yu, Y. Cai, and S. A. Ponomarenko, "Propagation of optical coherence lattices in the turbulent atmosphere," Opt. Lett. **41**, 4182–4185 (2016).
53. F. Wang, Y. Chen, L. Guo, L. Liu, and Y. Cai, "Complex Gaussian representations of partially coherent beams with nonconventional degrees of coherence," J. Opt. Soc. Am. A **34**, 1824–1829 (2017).
54. P. Meemon, M. Salem, K.-S. Lee, M. Chopra, and J. P. Rolland, "Determination of the coherency matrix of a broadband stochastic electromagnetic light beam," J. Mod. Opt. **55**, 2765-2776 (2008).
55. E. Wolf, "Can a light beam be considered to be the sum of a completely polarized and a completely unpolarized beam?" Opt. Lett. **33**, 642–644 (2008).
56. J. Tervo and J. Turunen, "Comment on "Can a light beam be considered to be the sum of a completely polarized and a completely unpolarized beam?" Opt. Lett. **34**, 1001 (2009).
57. E. Wolf, "Reply to Comment on "Can a light beam be considered to be the sum of a completely polarized and a completely unpolarized beam?"," Opt. Lett. **34**, 1002 (2009).
58. J. Tervo, J. Turunen, and F. Gori, "Impossibility of Stokes decomposition for a class of light beams," Opt. Commun. **283**, 4448–4451 (2010).
59. Q. Zhan, "Cylindrical vector beams: from mathematical concepts to applications," Adv. Opt. Photon. **1**, 1–57 (2009).
60. Q. Zhan and J. R. Leger, "Focus shaping using cylindrical vector beams," Opt. Express **10**, 324–331 (2002).
61. S. Chen, X. Zhou, Y. Liu, X. Ling, H. Luo, and S. Wen, "Generation of arbitrary cylindrical vector beams on the higher order Poincaré sphere," Opt. Lett. **39**, 5274–5276 (2014).
62. T. Stangner, H. Zhang, T. Dahlberg, K. Wiklund, and M. Andersson, "Step-by-step guide to reduce spatial coherence of laser light using a rotating ground glass diffuser," Appl. Opt. **56**, 5427–5435 (2017).
63. Y. Cai, Y. Chen, J. Yu, X. Liu, and L. Liu, "Generation of partially coherent beams," Prog. Opt. **62**, 157–223 (2017).
64. P. De Santis, F. Gori, G. Guattari, and C. Palma, "An example of Collet-Wolf source," Opt. Commun. **29**, 256–260 (1979).
65. D. Sarenac, D. G. Cory, J. Nsofini, I. Hincks, P. Miguel, M. Arif, Charles W. Clark, M. G. Huber, and D. A. Pushin, "Generation of a lattice of spin-orbit beams via coherent averaging," Phys. Rev. Lett. **121**, 183602 (2018).